Coarsening of the Sn-Pb Solder Microstructure in Constitutive Model-Based Predictions of Solder Joint Thermal Mechanical Fatigue[1]

P.T. Vianco
S.N. Burchett
M.K. Neilsen
J.A. Rejent

Sandia National Laboratories
Albuquerque, NM

D.R. Frear
Motorola Corp.
Phoenix, AZ

Abstract

An expression for the coarsening rate of the Pb-rich phase particles was determined through isothermal aging experiments and comparative literature data as:

$$\lambda = \lambda_o + \left\{[4.10\text{x}10^{-5}\, e^{-11023/T} + 15.6\text{x}10^{-8}\, e^{-3123/T}\, (d\gamma/dt)]t\right\}^{0.256}$$

where λ_o and λ are the initial and final mean Pb-rich particle diameters, respectively (mm); T is temperature (°K); t is time (s); and $d\gamma/dt$ is the strain rate (s^{-1}). The phase coarsening behavior showed good agreement with previous literature data from isothermal aging experiments. The power-law exponent, p, for the Pb-rich phase size coarsening kinetics:

$$\lambda^p - \lambda_o^p \approx t$$

increased from a value of 3.3 at the low aging temperature regime (70°C-100°C) to a value of 5.1 at the high temperature regime (135°C-170°C), suggesting that the number of short-circuit diffusion paths had increased with further aging. This expression provides an important basis for the microstructurally-based, constitutive equation used in the visco-plastic model for TMF in Sn-Pb solder. The revised visco-plastic model was exercised using a through-hole solder joint configuration. Initial data indicate a satisfactory compatibility between the constitutive equation and the coarsening expression.

Introduction

Thermal mechanical fatigue (TMF) is an important damage mechanism for solder joints exposed to cyclic temperature environments. Predicting the service reliability of

---

[1] Sandia is a multiprogram Laboratory operated by Sandia Corporation, a Lockheed Martin Company, for the United States Dept. of Energy under Contract DE-AC04-94AL85000.

solder joints exposed to such conditions requires two knowledge bases: First, the extent of fatigue damage incurred by the solder microstructure leading up to fatigue crack initiation, must be quantified in both time and space domains. Secondly, fatigue crack initiation and growth must be predicted since this metric determines, explicitly, the loss of solder joint functionality as it pertains to its mechanical fastening as well as electrical continuity roles.

This paper will describe recent progress in a research effort to establish a microstructurally-based, constitutive model that predicts TMF deformation to 63Sn-37Pb solder in electronic solder joints up to the crack initiation step[1,2]. The model is implemented using a finite element setting; therefore, the effects of both global and local thermal expansion mismatch conditions in the joint that would arise from temperature cycling.

The solder constitutive model mathematically describes the stress and deformation states in the solder as a function of the applied displacement and displacement rates. An important property of the present model is that it includes the parameter, λ, that pertains, explicitly, to the microstructural condition of the solder. This parameter is included in equation (1) below, which describes the magnitude of the inelastic deformation rate, $d\gamma_{in}/dt$.

$$d\gamma_{in}/dt = A\,[\exp(-Q/RT)]\,[\lambda_o/\lambda]^p\,[\sinh^m(\tau/\tau_o)] \qquad \text{Equation 1}$$

where A is a proportionality constant; Q is the apparent activation energy governing the deformation mechanism(s) in the solder; R is the universal gas constant; T is temperature; p and m are exponential constants; τ is the applied shear stress; and $\tau_o(\lambda_o,\lambda)$ is the flow stress. The parameters λ_o and λ represent the initial and current microstructural conditions respectively. The flow stress, τ_o, is also a function of the microstructural parameters, λ_o and λ, through equation (2) below:

$$\tau_o = \alpha\,[c + B(\lambda_o/\lambda)^E] \qquad \text{Equation 2}$$

The parameters α, B, and E are material constants. The state variable, c, captures the hardening/recovery processes and their effect on the flow stress of the material. The term $B(\lambda_o/\lambda)^E$ reflects the change to the flow stress caused by evolution of the microstructure. Therefore, equation (1) describing the deformation rate in the solder material is comprised of three principle terms: (1) the Arrhenius temperature dependence of the deformation mechanism, $[\exp(-Q/RT)]$; a microstructure term, $[\lambda_o/\lambda]^p$; and the stress term, $[\sinh^m(\tau/\tau_o)]$, which is also dependent on the solder microstructure through τ_o.

The implementation of this model requires the selection of a microstructural feature that is predominant in the constitutive behavior of the Sn-Pb solder. It has long been recognized that TMF of 63Sn-37Pb eutectic and near-eutectic solders is *accompanied by* a coarsening of the Pb-rich phase particles. This phenomenon is illustrated in Fig. 1 which shows TMF damage in a connector solder joint subjected to temperature cycling. Therefore, the Pb-rich phase particle size was established as the microstructural metric for TMF deformation in Sn-Pb solder. Again, the microstructural parameters λ_o and λ in the constitutive equation represent the initial and current, mean Pb-rich phase particle size, respectively. It is assumed that the Pb-rich phase particles were spherical so that the microstructural parameter, λ, is the mean diameter of the particles.

Coarsening of the Pb-rich phase particles during TMF can be considered as being comprised of two contributory factors. First, there is thermally activated particle growth caused solely by elevated temperature conditions; this process is referred to as *static coarsening* in following discussions. The second factor is an enhancement of the coarsening process caused by the applied strain or deformation; this process is referred to as *dynamic coarsening*.

Clark and Alden investigated the coarsening kinetics of single phase materials[3]. That work assumed that grain size coarsening, $d\lambda/dt$, was inversely proportional to the grain size:

$$d\lambda/dt \approx M(1/\lambda) \qquad \text{Equation 3}$$

where M is the mobility of the diffusing species. In this theory, the diffusion species was vacancies. The differential equation reduces to an integral form of:

$$\lambda^2 - \lambda_o^2 = Kt \qquad \text{Equation 4}$$

where K is a constant that includes an Arrhenius temperature dependence. This equation suggests that the bulk diffusion of vacancies is the predominant mechanism.

Other coarsening laws have also been developed. Lifshitz and Slyozov derived a coarsening law for single phase materials that was based upon the grain size raised to a third power[4]. The mathematical equation is:

$$\lambda^3 - \lambda_o^3 = [(c_1/T)\exp(\Delta H/RT)]t \qquad \text{Equation 5}$$

where c_1 is a constant; ΔH is the activation energy for volume diffusion between grains; R is the universal gas constant; and T is temperature. Snekov and Myschlyaev modified

this theory in order to describe the coarsening of second phase particles located on grain boundaries[5]. In this instance, coarsening is described by the following equation:

$$\lambda^4 - \lambda_o^4 = B_2[\gamma_o \Omega C_o \delta D_b / RT]t \qquad \text{Equation 6}$$

where B_2 is a geometric constant; γ_o is the interfacial energy and the primary driving force for coarsening; Ω is the molar volume of second phase; C_o is solute concentration on the grain boundaries; δD_b is the grain boundary diffusivity (thermally activated); R is the universal gas constant; and T is temperature. This theory is based upon grain boundary diffusion processes as the active mechanism in support of coarsening. These theories must be interpreted against the coarsening behavior of Sn-Pb solder.

A study by Hacke, Sprecher, and Conrad investigated the static coarsening kinetics of the Pb-rich phase under isothermal annealing conditions using three aging temperatures, 85°C, 130°C, and 150°C, and three time periods between 1 and 60 hrs[6]. Those particle size data were fit to the power law similar to equation 5 above. The apparent activation energy, ΔH, was calculated to be 29 kJ/mol. Those same data were later fit to an expression similar to equation 6 which expresses the phase size to a fourth order power law[7,8]. The value of ΔH was calculated to be 40 kJ/mol. Clearly, some ambiguity persists as to how to best represent the coarsening kinetics of the Pb-rich phase in Sn-Pb solder.

It is necessary to have an accurate description of the Pb-rich phase coarsening kinetics in order for the microstructurally-based, constitutive model to provide a reliable prediction of TMF deformation. Therefore, the following, more generalized approach was taken. First, as in the Clark-Alden model, it was assumed that the *static* coarsening rate of the Pb-rich particles is controlled by the equilibrium concentration of vacancies in the microstructure, v_o. The value of v_o is dependent upon temperature. Secondly, it was presumed that the coarsening rate can be accelerated beyond the static rate when there are excess vacancies, v_x, in the microstructure. Excess vacancies are assumed to be generated when the material is exposed to deformation processes. The quantitative analysis begins with the generalized form of equation 3 presented below:

$$d\lambda/dt = (MA_1)/\lambda^p \qquad \text{Equation 7}$$

where M is the vacancy mobility and A_1 is a temperature-dependent, material parameter. The microstructural parameter λ is raised to the power, p; no particular value for p is presumed. The mobility parameter, M, is represented as:

$$M = D_v(v_o + v_x)/kT \qquad \text{Equation 8}$$

where D_v is the diffusion coefficient of vacancies, $(v_o + v_x)$ is the total number of vacancies in the microstructure, and kT is the product of the Boltzmann constant and absolute temperature. Combining equations 7 and 8 results in the following expression:

$$d\lambda/dt = [D_v A_1/kT] [(v_o + v_x)/\lambda^p] \qquad \text{Equation 9}$$

This equation is modified by establishing a temperature-dependent parameter A_2 to represent the coefficient; that is:

$$d\lambda/dt = A_2 (v_o + v_x)/\lambda^p \qquad \text{Equation 10}$$

The vacancy concentration in equation 10 is analyzed in further detail. The change in total vacancy concentration, $d(v_o+v_x)/dt$, is simply the change in excess vacancies, dv_x/dt. In turn, the rate of change of excess vacancies is a result of the net balance between the rate of excess vacancy production and rate of excess vacancy annihilation. The rate of vacancy production is assumed to be proportional to the strain rate, $d\gamma/dt$; the rate of annihilation is assumed to be proportional to the instantaneous, excess vacancy concentration, v_x[3]:

$$dv_x/dt = A_3(d\gamma/dt) - A_4 v_x. \qquad \text{Equation 11}$$

The parameter A_3 was estimated to be constant at 1.7×10^{-5}, using the work of Barry and Brown[9]. The equation for the parameter A_4 was derived in Reference 1:

$$A_4 = (1.94 \times 10^{13}) \exp(-7.9 \times 10^3/T) \qquad \text{Equation 12}$$

The parameter, A_4, has units of s^{-1}. The integration of equation 11 results in equation 13 for the excess vacancy concentration, v_x, at time t:

$$v_x = (A_3/A_4) (d\gamma/dt) [1-\exp(-A_4 t)] \qquad \text{Equation 13}$$

It was assumed that the *excess* vacancy concentration at the start of deformation (t=0), $v_{x,o}$, was equal to zero. Given the parameters contained in the expression for A_4 (equation 12), it was observed that, for all anticipated times, t, equation 13 reduces to:

$$v_x \approx (A_3/A_4)\, d\gamma/dt \qquad \text{Equation 14}$$

Therefore, the rate equation for Pb-rich phase coarsening can be simplified into the following format:

$$d\lambda/dt = A_2 [v_o + (A_3/A_4)\, d\gamma/dt]/\lambda^p \qquad \text{Equation 15}$$

The coarsening rate described by equation 15 can be considered as being comprised of two contributions, the static coarsening rate, $d\lambda/dt]_s$, and the dynamic coarsening rate, $d\lambda/dt]_d$ as described by equations 16 and 17 below:

$$d\lambda/dt]_s = A_2\, v_o/\lambda^p \qquad (d\gamma/dt = 0) \qquad \text{Equation 16}$$

$$d\lambda/dt]_d = A_2\, (A_3/A_4)(d\gamma/dt)/\lambda^p \qquad \text{Equation 17}$$

At this point, static aging experiments would be used to determine values for the parameters, $(A_2 v_o)$ and p. Assuming a value for v_o from the literature source, A_2 can be computed. Then, the dynamic term for phase coarsening can be completed, given the literature value for A_3 and equation 12 that predicts A_4.

A slightly different mathematical format to equation 16 was believed to better represent the experimental coarsening data for static aging conditions. The phenomenological expression having the following form was used:

$$\lambda - \lambda_o = A\, t^n \exp(-\Delta H/RT) \qquad \text{Equation 18}$$

where A is a constant; nis the time exponent (which is also a consta nt); and ΔH is the apparent activation energy for the coarsening process. All other symbols are as defined previously. The differential form of Equation 18 can be can be rearranged into a form equivalent to equation 16:

$$d(\lambda - \lambda_o)/dt]_s = d\lambda/dt]_s = \frac{n[(A\exp(-\Delta H/RT)]^{1/n}}{(\lambda - \lambda_o)^{(1/n)-1}} \qquad \text{Equation 19}$$

In this format, the parameters in equation 16 are calculated as follows:

$$p = (1/n) - 1 \qquad \text{Equation 20}$$

and $$A_2 v_o = n[(A\exp(-\Delta H/RT)]^{1/n}$$ Equation 21

The equations 18 and 19 predict the static coarsening of the Pb-rich phase particles. In TMF, the dynamic contribution to the overall phase coarsening must also be taken into account. Starting with equation 19, it was assumed that the dynamic term will have the same phase size dependence (i.e., denominator) as does the right-hand side of equation 19:

$$d\lambda/dt = \frac{A_2 v_o}{(\lambda - \lambda_o)^{(1/n)-1}} + \frac{f(d\gamma/dt, T)}{(\lambda - \lambda_o)^{(1/n)-1}}$$ Equation 22

The stipulation that the dynamic term has the same phase size dependence (denominator) as does the static term is based upon the premise that the sole role of the deformation is to increase the number of vacancies in the microstructure. That is, deformation has no explicit role in the diffusion of those excess vacancies nor any other mechanism that directly impacts the actual Pb-rich phase coarsening rate kinetics. Next, the expression, $f(d\gamma/dt, T)$, was taken to be equivalent to the coefficient in equation 17:

$$f(d\gamma/dt, T) = A_2(A_3/A_4)(d\gamma/dt)$$ Equation 23

The temperature dependence of the dynamic coarsening contribution is a result of the combined temperature dependencies of vacancy motion (through A_2) and vacancy annihilation (through A_4). Therefore, the rate Pb-rich phase particle coarsening is described by the following generalized equation:

$$d\lambda/dt = \frac{A_2 v_o}{(\lambda - \lambda_o)^{(1/n)-1}} + \frac{[A_2(A_3/A_4)(d\gamma/dt)]}{(\lambda - \lambda_o)^{(1/n)-1}}$$ Equation 24

The logistics for determining the coefficients in equation 24 are as follows:

(1) Perform isothermal aging experiments to determine A, n, and ΔH in the equation:

$$\lambda - \lambda_o = A\, t^n \exp(-\Delta H/RT).$$

(2) Compute the value of A_2v_o from the experimental results, using the following expression:

$$A_2v_o = n[(A\exp(-\Delta H/RT)]^{1/n}.$$

(3) Calculate A_2, assuming a literature value of v_o:

$$v_o = 1 \times 10^{-9}$$

(4) Incorporate literature values for A_3 and A_4 into the equation:

$$A_3 = 1.7 \times 10^{-5}$$

$$A_4 = 1.9 \times 10^{13} \exp(-7900/T) \ /s$$

The Pb-rich phase coarsening predicted by equation 24 was compared against available literature results.

The constitutive model was modified to include the revised expression for coarsening of the Pb-rich phase size, Equation 24. The model was then used to predict TMF deformation in the Sn-Pb solder microstructure of several through-hole solder joint configurations; an initial example of these calculations is provided, and confirmed the compatibility of the new expression with the overall model.

Experimental Procedures

Pb-rich phase size coarsening.

Test samples used to determine the static coarsening kinetics for the Pb-rich phase size were fabricated by the following procedures. Oxygen-free, high conductivity (OFHC) Cu substrates were formed with the dimensions of 6.35 x 6.35 x 1.59 mm. The sample was immersed into a bath of molten 63Sn-37Pb solder (215°C) for 5 s and withdrawn so as to allow the polished surface to exit the bath last and parallel to the solder surface. This procedure allowed a large volume of solder to accumulate on that surface which was used for the Pb-rich phase size measurements. It was presumed that any residual stresses that may have developed in the solder, such as those caused by thermal expansion mismatch between the solder film and Cu substrate, were quickly relieved early in the respective aging treatments and thus, did not significantly impact the coarsening process(es).

Individual specimens were thermally aged in air furnaces having a temperature stability of $\pm$1°C. The aging temperatures were 70°C, 100°C, 135°C, and 170°C. The aging times ranged from 1 day to 400 days and were within $\pm$30 min of the nominal time interval. After the aging treatment had been completed, each specimen was cross-sectioned, mounted, and polished for metallographic viewing. An as-fabricated sample was also evaluated.

Pb-rich phase sizes were measured with the following steps. Two 500x optical micrographs were taken within the solder field of the sample. An established, quantitative image analysis routine was developed, with which to determine the following parameters for the Pb-rich particles: (1) mean area (size), (2) standard deviation, (3) maximum area, (4) number of particles counted, and (5) the total Pb-rich phase present in the evaluated area. Although the fifth parameter of total Pb-rich phase present in the viewed area was not critical to the actual particle size analysis, it was monitored to verify that the selected viewing area (magnification) represented the overall Pb content in the sample. Too high a magnification captured very small particles, but also increased the chances of inaccurate particle counts in the micrographs. This condition would have necessitated a considerably large number of viewing areas. On the other hand, too low a magnification caused the smaller particles to be omitted from the count.

The data from each of the two evaluated areas were combined. The distribution of Pb-rich phase particle sizes were initially obtained as particle "areas", A. The "area" data were then converted to particle diameters (D) by assuming that the particles were spherically shaped ($D=2\sqrt{[A/\pi]}$). The as-fabricated condition was $D_o=2.257x10^{-3}$ mm (2.257 μm).

Results and Discussion

Coarsening of the Pb-rich phase size

The extent of coarsening is illustrated by the photomicrographs in Fig. 2. The micrograph in Fig. 2a was taken of the as-fabricated specimen. Some spheroidization of the Pb-rich phase has occurred. However, there remains a large number of areas showing the lamellae cell structure. Shown in Fig. 2b is a micrograph of the sample aged at 100°C for 350 days. Complete spheroidization of the Pb-rich particles has occurred. The size of the particles has clearly increased and their number, diminished, as a result of the aging treatment. The log-normal distribution of particle sizes that was identified by the image analysis, is illustrated by the histograms in Fig.3. These *particle area* data were obtained from a single, 500x micrograph of the sample aged at 100°C for 6 days. Listed in Table 1 are (1) the mean particle size (diameter) values, (2) the particle size standard deviations, and (3) the number of particles analyzed per each of the heat treatment conditions. There was a large variation in particle size per each field-of-view as is reflected by the standard deviation values. The mean particle size was used in the static aging kinetics determination for the constitutive model.

A multiple linear regression analysis was used to determine the pre-exponential constant, A; the time exponent, n; and the apparent activation energy, ΔH, for the application of equation 18. The analysis was performed on the logarithm of equation 18, using commercial statistics software:

$$\ln(\lambda - \lambda_o) = \ln A + n\ln t - \Delta H/RT \qquad \text{Equation 25}$$

The time, t, and reciprocal temperature, 1/T, were the independent variables while $\ln(\lambda - \lambda_o)$ served as the dependent variable. As noted, the value of λ_o representing the as-fabricated, mean particle diameter was 2.257×10^{-3} mm. Three regression analyses were performed, each being distinguished by the aging temperature regimes: (1) "low-temperature aging," 70°C and 100°C; (2) "high-temperature aging," 135°C and 170°C; and (3) the entire temperature range of 70°C through 170°C. Shown in Fig. 4a is a plot of the mean particle size data points as a function of aging time and temperature. The accompanying curves were calculated from the linear regression analysis that used data covering the entire 70-170°C temperature regime. The corresponding log-log plot pertaining to equation 25 is shown in Fig. 4b.

The kinetics parameters that were calculated from the isothermal aging data are listed in Table 2. It was observed that the apparent activation energy remained relatively unchanged between the temperature regimes. However, the time exponent decreased as the aging temperature increased, from a value of 0.299 (70°C, 100°C) to 0.195 (135°C, 170°C). The power-law in time exponent, n, used in equation 18 was converted to the exponent, p, found in equation 16, using equation 20. Three expressions were written per each of the temperature regimes, based upon the integration of equation 16:

$$\lambda^{3.3} - \lambda_o^{3.3} \approx t \qquad 70°C,\ 100°C \qquad \text{Equation 26a}$$

$$\lambda^{5.1} - \lambda_o^{5.1} \approx t \qquad 135°C,\ 170°C \qquad \text{Equation 26b}$$

$$\lambda^{3.9} - \lambda_o^{3.9} \approx t \qquad 70 - 170°C \qquad \text{Equation 26c}$$

The values of the power-law exponents in equations 26a through 26c were considerably greater than the value of two (2) associated with bulk diffusion mechanisms (or n=0.5 in equation 18 under the same premise). Short-circuit diffusion paths caused by the interphase boundaries between the Pb-rich and Sn-rich phases have been hypothesized. However, the kinetics parameters in equations 26a-26c do not entirely support this notion. The particle size exponent increased from the lower to the higher temperature regimes. As the Pb-rich phase size increased, the extent of Pb-rich phase boundary area would decrease. Thus, there would be a reduction in the extent of short-circuit diffusion, possibly in favor of a predominance by bulk diffusion processes. Under this latter scenario, the power-law exponent for particle size would be expected to decrease towards the traditional value of two (2) at the higher aging temperatures. The data presented in equations 26a-26c suggests, in fact, that the isothermal aging may have *increased* the number of fast-diffusion paths in the solder microstructure.

Lastly, it was observed that the calculated apparent activation energy derived from the present data, 23.5 kJ/mol (70-170°C), was considerably less than that cited for bulk diffusion through either Sn (94 kJ/mol) or Pb (101 kJ/mol)[10]. The low value of the apparent activation energy suggests that short-circuit, diffusion mechanisms supported the Pb-rich phase particle coarsening in the Sn-Pb solder. Also, the fact that the apparent activation energy was relatively insensitive to the temperature regimes implies that the fundamental mechanism responsible for fast-diffusion had not changed as the phase size increased with aging. Rather, the isothermal aging treatments simply increased the number of short-circuit paths. These observations imply that the coarsening of the Pb-rich phase particles may actually be determined by diffusion mechanisms associated with the Sn-rich matrix rather than solely with Pb-rich phase boundaries.

The computed kinetics parameters representing the entire70-170°C temperature regime were introduced into the coarsening equation 24:

$$d(\lambda - \lambda_o)/dt = \frac{1.05\times10^{-5}\, e^{-11023/T}}{(\lambda - \lambda_o)^{2.9}} + \frac{9.47\times10^{-15}\, e^{-3123/T}\,(d\gamma/dt)}{(\lambda - \lambda_o)^{2.9}} \qquad \text{Equation 27}$$

where the particle diameter, λ, is in mm; the temperature, T, is in °K; and time (t) is in seconds. The integral form of equation 27, which calculates the Pb-rich phase particle size, is given as equation 28 below:

$$\lambda = \lambda_o + \left\{[4.10\times10^{-5}\, e^{-11023/T} + 3.69\times10^{-14}\, e^{-3123/T}\,(d\gamma/dt)]t\right\}^{0.256} \qquad \text{Equation 28}$$

A confirmation of the accuracy of this function was made by comparing the computed particle diameters using equation 28 against values measured in the study by Hacke, Sprecher, and Conrad following *static* aging ($d\gamma/dt = 0$) at 85°C, 135°C, and 150°C [8]. This comparison is illustrated in Fig. 5. Excellent agreement was observed. This agreement was particularly satisfying from the viewpoint of the predictive capabilities exhibited by the static term in equation 28. That is, the isothermal aging experiments used to develop the static aging contribution in equation 28 spanned several thousands of hours. Yet, the function was able to accurately predict particle coarsening for time periods of 60 hours or less.

However, when *both* static and dynamic coarsening effects were considered, as would be the necessary for modeling TMF deformation, the particle size predicted by equation 28 and that measured in the aforementioned work were not in agreement. Therefore, the coefficient, 3.69×10^{-14}, in equation 27 was adjusted so that the predicted phase size matched that of the experimental TMF data. The exponential term was not altered. A satisfactory curve fit was realized when the magnitude of the coefficient term

was reduced by nearly six orders, to a value of 15.6×10^{-8}. The predicted Pb-rich phase size and the cited data are also illustrated in Fig. 5. Therefore, the modified equation that better represents the coarsening behavior of the Pb-rich phase is:

$$\lambda = \lambda_o + \left\{ [4.10 \times 10^{-5} e^{-11023/T} + 15.6 \times 10^{-8} e^{-3123/T} (d\gamma/dt)]t \right\}^{0.256} \quad \text{Equation 29}$$

Computational exercise – plated through hole solder joint

A preliminary assessment was made of the compatibility of the revised coarsening expression with the inelastic deformation rate equation, and exercising the latter function in the execution of the model. A computational "quarter symmetry" geometry was developed for a plated-through hole solder joint; that geometry is shown in Fig.6. The laminate material was FR-4 and measured 1.6 mm thick. The hole diameter was 0.91 mm. The lead material was Cu and had a diameter of 0.51 mm. The configuration of the solder fillet was a replication of that observed in an actual solder joint and was subsequently mapped into the model. The leads were attached to a ceramic base-material resistor. The temperature cycle was from –55°C to 125°C. The hold time at the temperature limits was 10 min. The entire cycle duration was 1 hour. The initial Pb-rich phase size was 2.257×10^{-3} mm.

Shown in Fig. 7 is a map of the Pb-rich phase size in the solder joint fillet after the completion of 2 cycles. The maximum mean Pb-rich particle size was computed to be 3.6×10^{-3} mm, which was located in the fillet, near the lead at the mouth of the hole on the component side of the circuit board. The minimum particle size of 2.8×10^{-3} mm was observed in the hole interior, near the center line of the laminate. The latter coarsening magnitude represents largely the effects of the temperature environment as well as the z-expansion mismatch between the laminate and the lead. A determination that the magnitude of the observed phase coarsening awaits the outcome of temperature cycling experiments that are currently underway on actual hardware.

Conclusions

1. Refinements were made to the microstructurally-based, constitutive equation used in the visco-plastic model for TMF deformation in the eutectic Sn-Pb solder.

2. Specifically, a new expression for the coarsening rate of the Pb-rich phase particles was determined through isothermal aging experiments.

3. The predicted static contribution to the phase coarsening behavior corroborated literature data. That same data was used to adjust the magnitude of the dynamic (strain-enhanced) contribution to the coarsening expression.

4. The power-law exponent for the Pb-rich phase size increased from the lower-to-high aging temperature regimes. This trend suggests that short-circuit diffusion paths had increased with added aging, and that the Pb-rich phase size boundaries were not the sole source of such fast diffusion pathways.

5. The visco-plastic model having the revised coarsening law was exercised using a through-hole solder joint configuration. Initial data indicate a satisfactory compatibility between the constitutive equation and the coarsening expression. Validation of the predicted microstructural evolution awaits the completion of current experiments.

Acknowledgements

The authors wish to thank Alice Kilgo for preparation of the metallographic samples and Eliot Fang for his careful review of the manuscript.

References

[1] D. Frear, S. Burchett, and M. Neilsen, *Adv. In Elect. Pack.* EEP-Vol. 19-2, (1997).

[2] S. Burchett, M. Neilsen, D. Frear, and J. Stephens, *Design and Reliability of Solders and Solder Interconnects* ed. by R. Mahidhara, et al., (TMS Warrendale, PA; 1997), p. 171.

[3] M. Clark and T. Alden, *Acta Met* 21 1195 (1973).

[4] M. Lifshitz and V. Slyozov, *J. Phys. Chem. Solids,* 19 35 (1961).

[5] O. Senkov and M. Myschlyaev, *Acta Metall.* 34 97 (1986).

[6] P. Hacke, A. Sprecher, and H. Conrad, *J. Electr. Pack.* 115 153 (1993).

[7] P. Hacke, A. Sprecher, and H. Conrad *J. Electronic Mater.* 26 774 (1997).

[8] P. Hacke, Y. Fahmy, and H. Conrad *J. Electronic Mater.* 27 941 (1998).

[9] B. Barry and A. Brown, *Acta Met.* 12 209 (1964).

[10] J. Askin, *Tracer Diffusion Data* (New York, NY Plenum. 1970).

Figures

Fig. 1 Optical micrographs showing the coarsening of the microstructure in a connector solder joint having undergone temperature cycling.

Fig. 2 Optical micrographs illustrating the coarsening of the Pb-rich phase particles in 63Sn-37Pb samples under static aging conditions: (a) as-fabricated condition and (b) aged at 100°C for 350 days.

Fig. 3 Histograms showing the distribution of Pb-rich phase particle sizes (projected area) for the sample static aged at 100°C for 6 days: (a) 0-2x10^{-5} mm^2 in bins of 2x10^{-6} mm^2 and (b) 0-2x10^{-6} mm^2 in bins of 2x10^{-7} mm^2. The mean particle diameter was 3.10 μm; the standard deviation was 3.86 μm; the maximum particle diameter was 15.1 μm; and the total number of particles in the analysis was 3147 (two areas).

Fig. 4 Isothermal aging data: (a) mean particle diameter as a function of aging time and (b) the plot of $\ln(\lambda-\lambda_o)$ as a function of ln(t).

Fig. 5 Plot of Pb-rich particle size data from isothermal and TMF fatigue experiments performed by Hacke, et al, and curves predicted by the empirical equation for phase coarsening.

Fig. 6 Computational geometry of the plated through-hole solder joint configuration used to evaluate the revised constitutive model. The printed wiring board laminate is FR-4 (1.6 mm thick); the lead material is Cu (0.51 mm diameter); and the device body is ceramic. The hole diameter is 0.91 mm.

Fig. 7 Map of the mean Pb-rich phase particle size as a function of the position within the through-hole solder joint after two thermal cycles (-55°C – 125°C; 10 min holds at limits; and 1 hour cycle). The location of greatest coarsening is marked. The starting Pb-rich phase particle diameter was 2.257x10^{-3} mm.

Tables

Table 1 Pb-rich Phase Particle Size Statistics Following Static Aging Treatments

Table 2 Experimental Static Aging Kinetics Parameters per Temperature Category

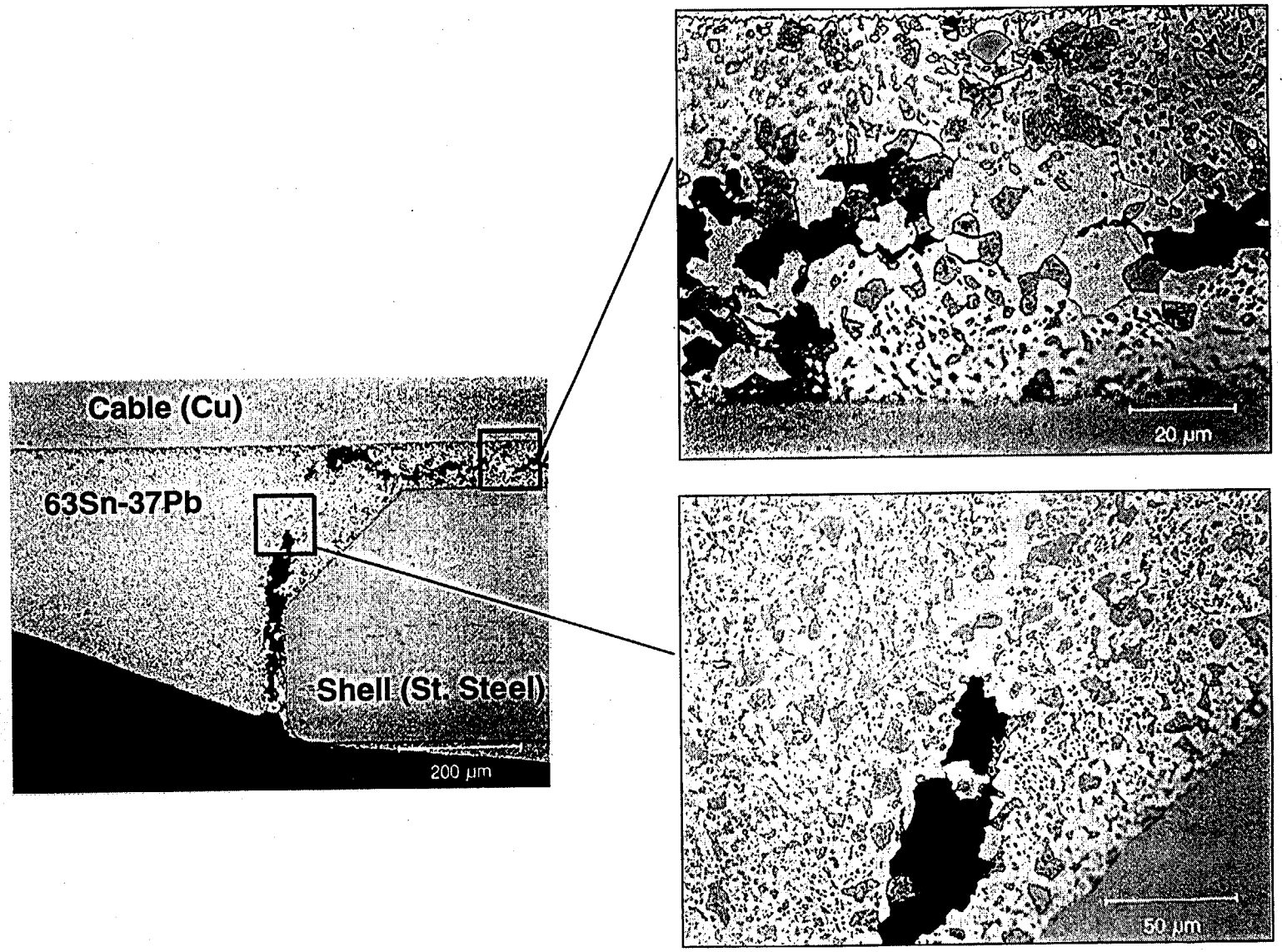

Fig. 1

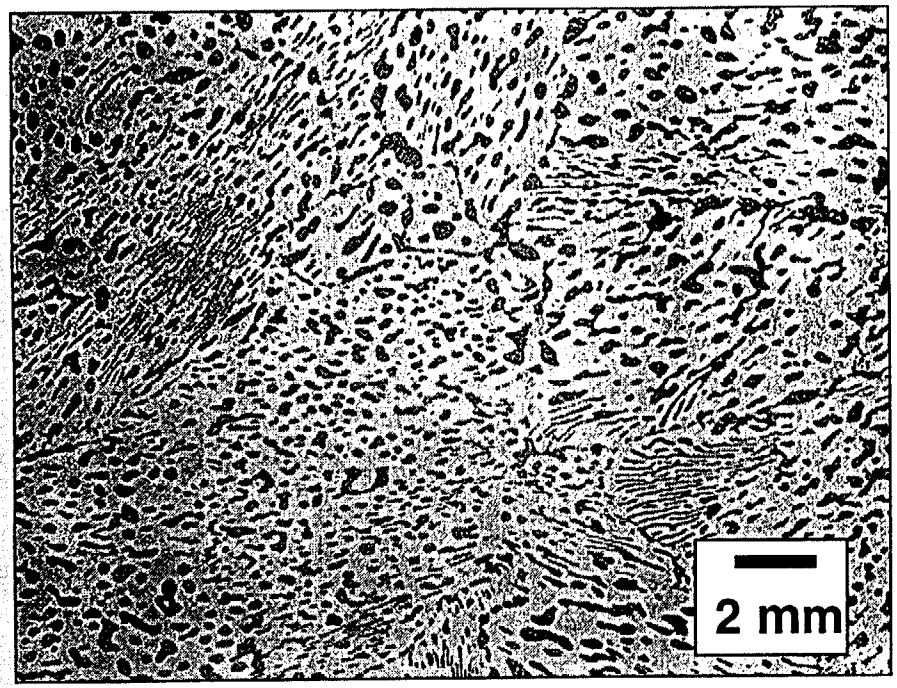

(a)

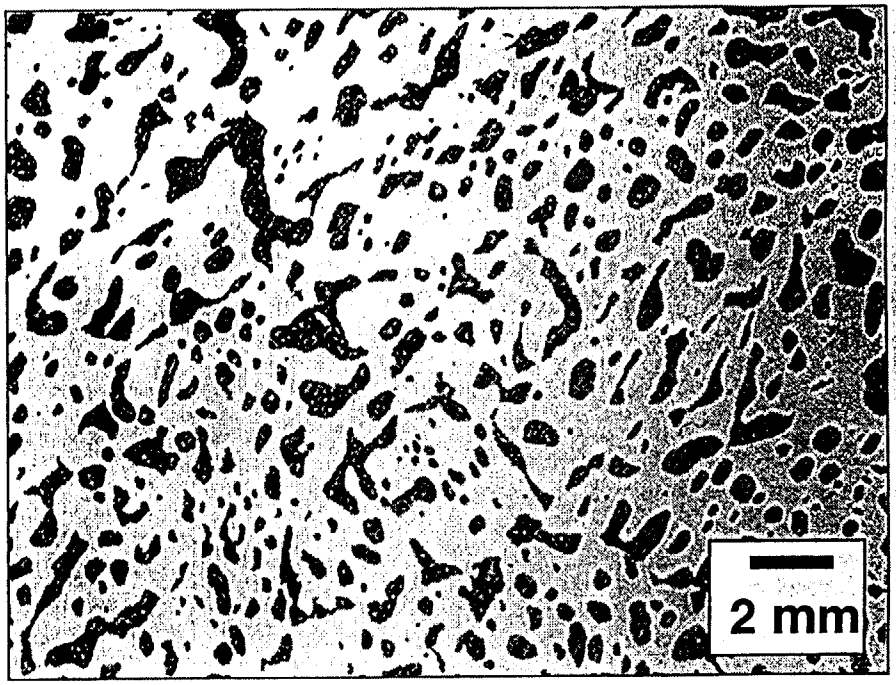

(b)

Fig. 2

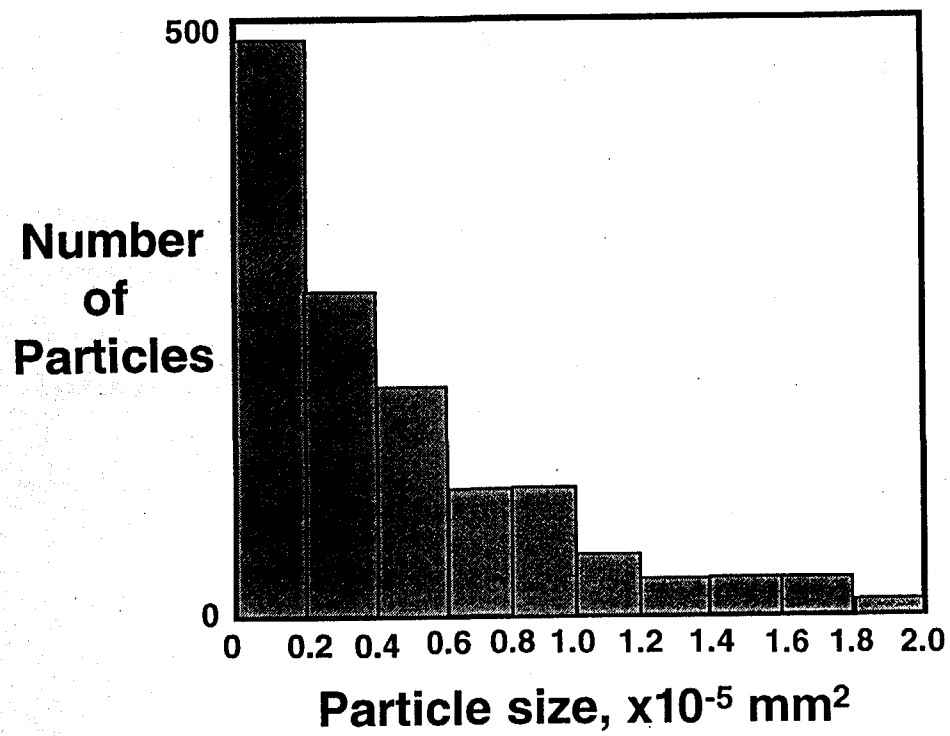
500
Number
of
Particles
0
0 0.2 0.4 0.6 0.8 1.0 1.2 1.4 1.6 1.8 2.0
Particle size, x10-5 mm2

(a)

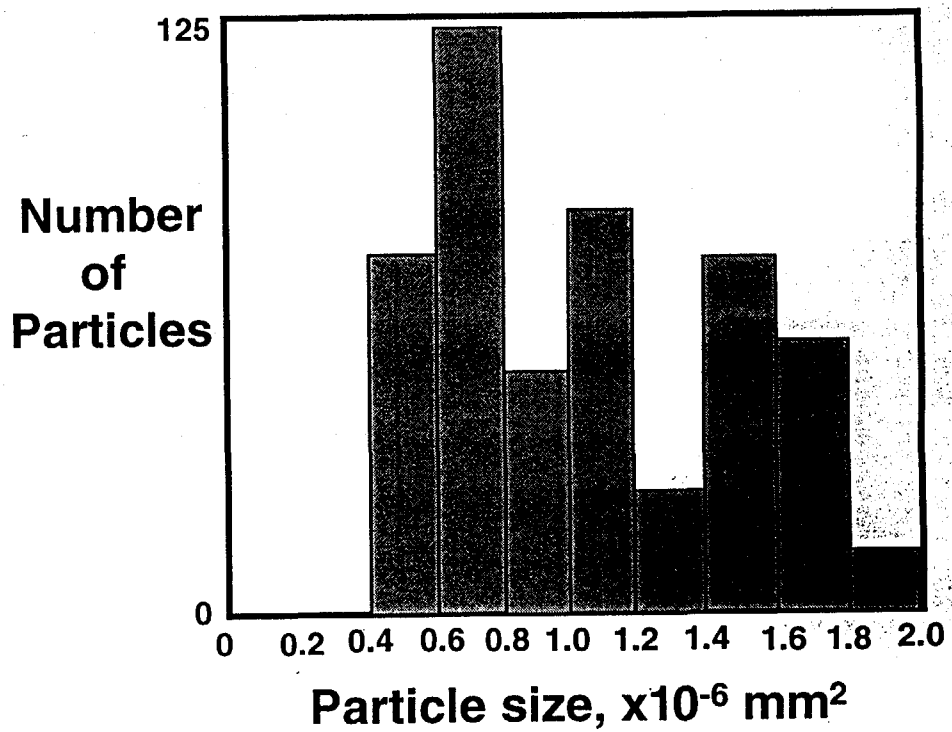
125
Number
of
Particles
0
0 0.2 0.4 0.6 0.8 1.0 1.2 1.4 1.6 1.8 2.0
Particle size, x10-6 mm2

(b)

Fig. 3

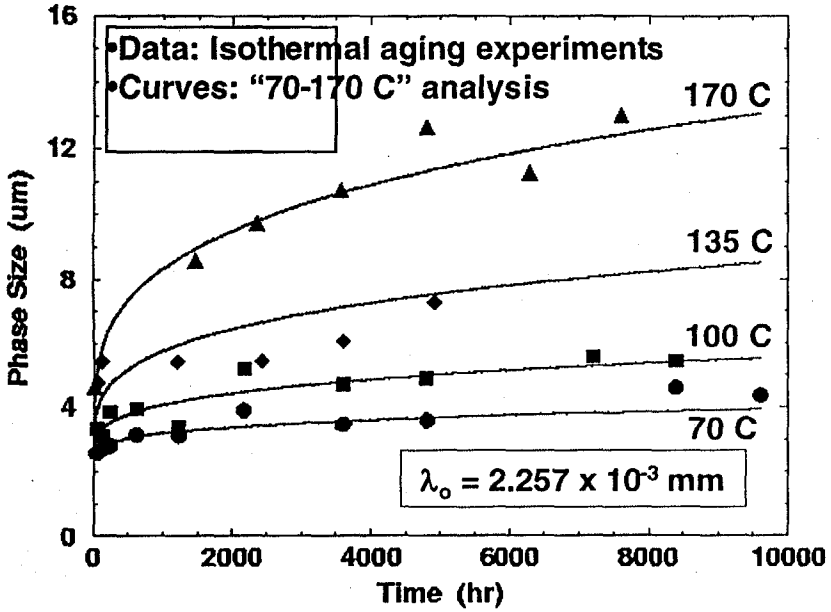
•Data: Isothermal aging experiments
•Curves: "70-170 C" analysis
170 C
135 C
100 C
70 C
λo = 2.257 x 10-3 mm
Phase Size (um)
Time (hr)
0
4
8
12
16
0
2000
4000
6000
8000
10000

(a)

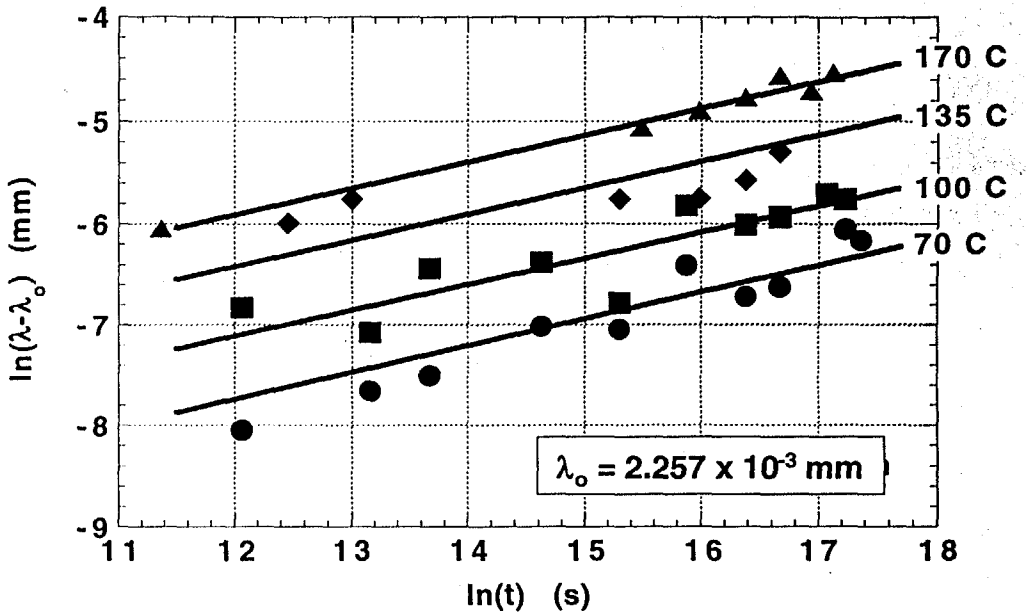
170 C
135 C
100 C
70 C
λo = 2.257 x 10-3 mm
ln(λ-λo) (mm)
ln(t) (s)
-4
-5
-6
-7
-8
-9
11
12
13
14
15
16
17
18

(b)

Fig. 4

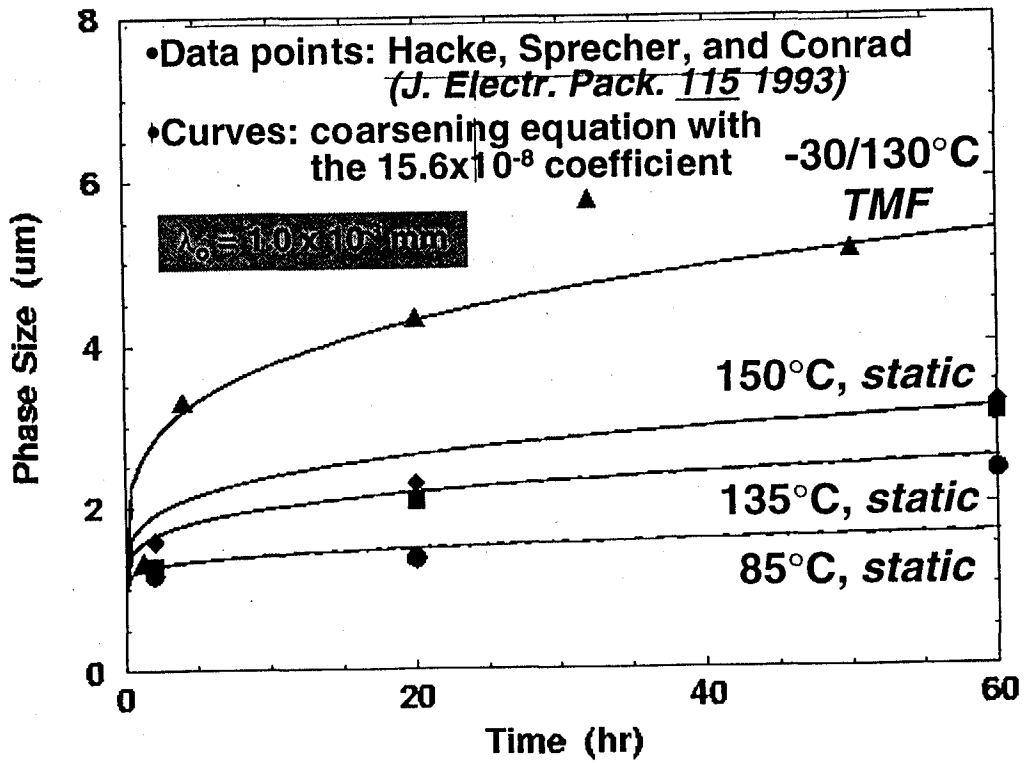
•Data points: Hacke, Sprecher, and Conrad
(J. Electr. Pack. 115 1993)
•Curves: coarsening equation with
the 15.6x10-8 coefficient
-30/130°C
TMF
150°C, static
135°C, static
85°C, static
Phase Size (um)
Time (hr)
0
2
4
6
8
0
20
40
60

Fig. 5

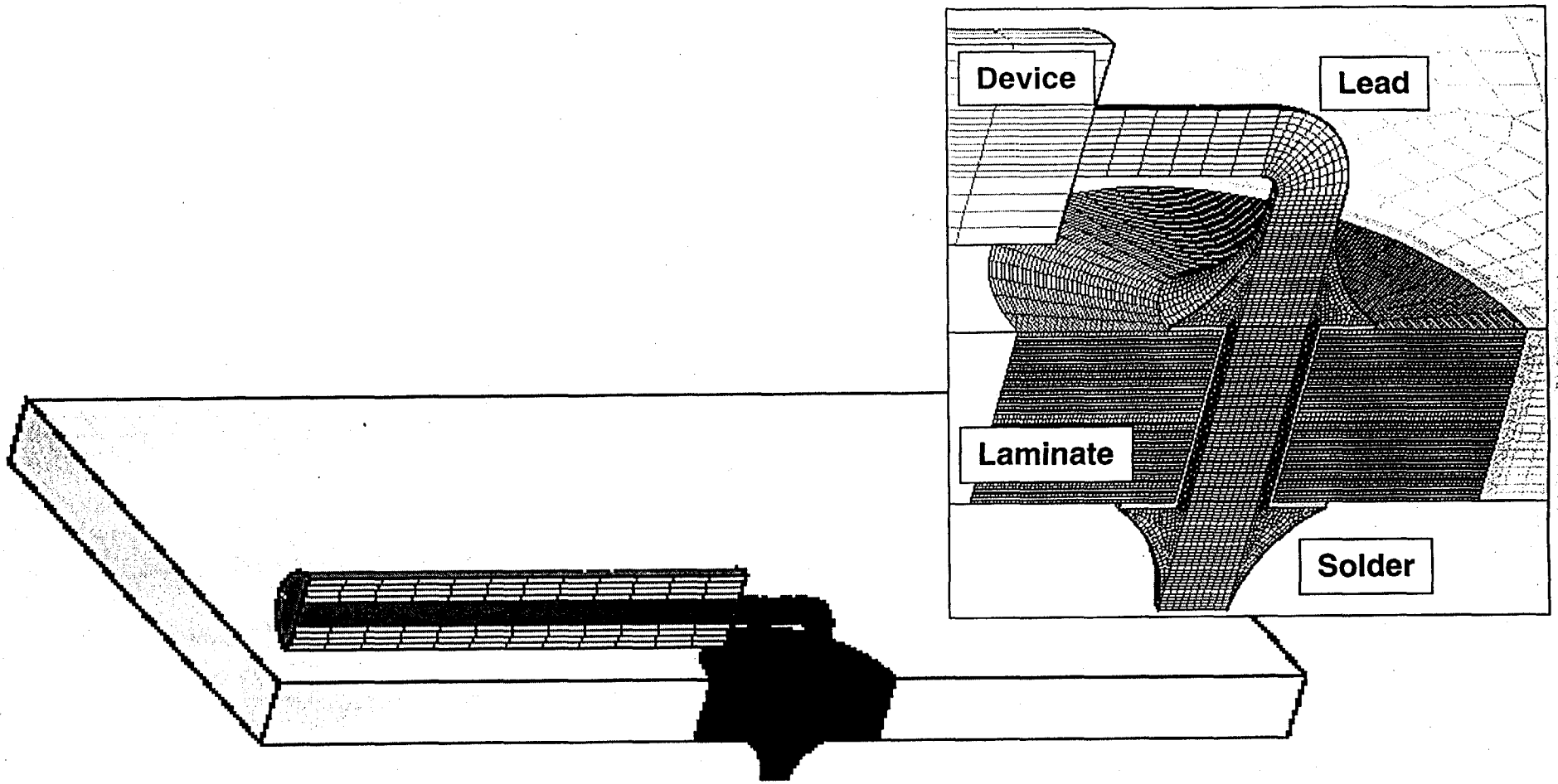

Fig. 6

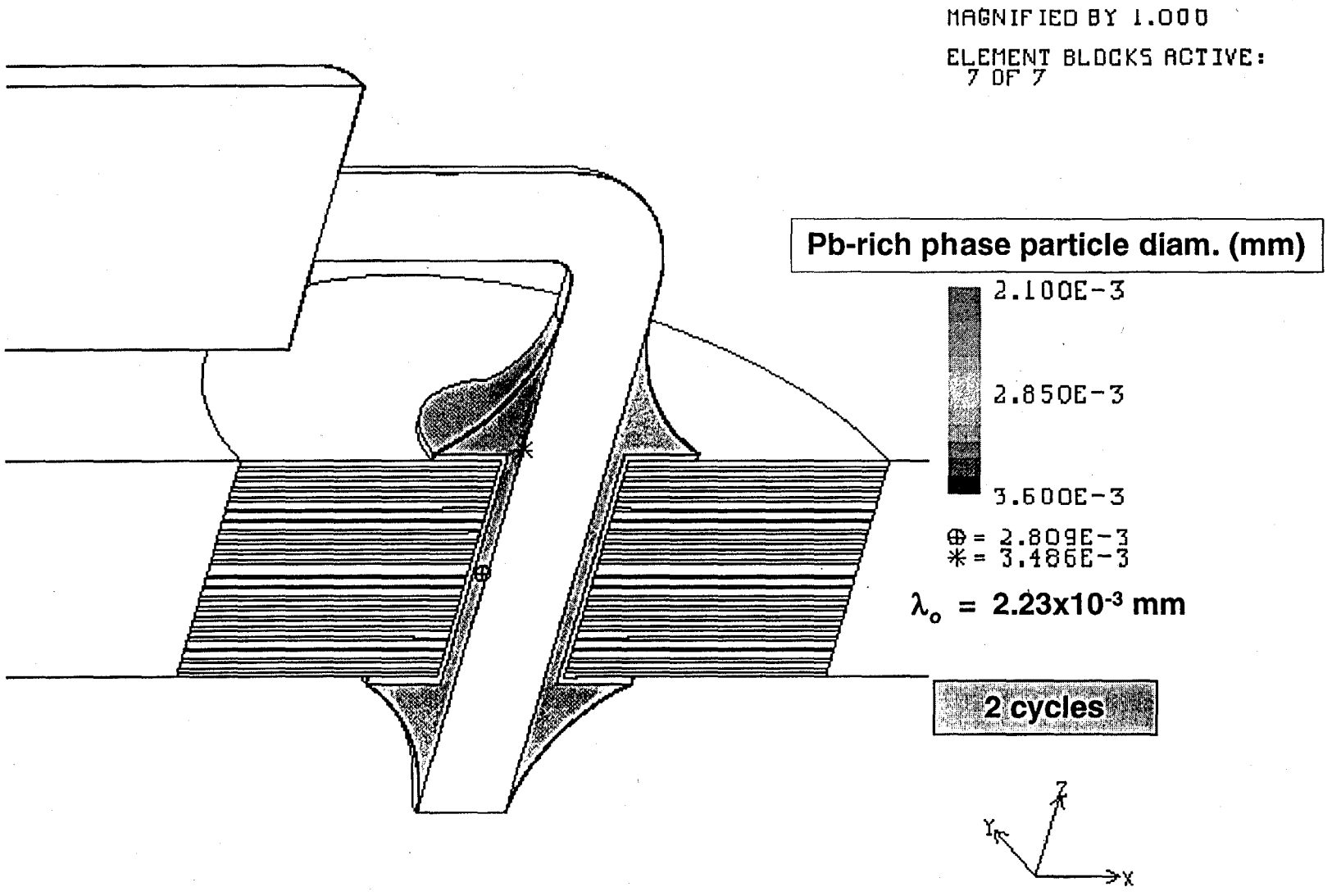
MAGNIFIED BY 1.000
ELEMENT BLOCKS ACTIVE:
7 OF 7
Pb-rich phase particle diam. (mm)
2.100E-3
2.850E-3
3.600E-3
⊕ = 2.809E-3
✳ = 3.486E-3
λ_o = 2.23x10^{-3} mm
2 cycles
Z
Y
X

Fig. 7

Aging Temp. (C)	Aging Time (days)	Mean Pb-rich phase particle diameter, l (mm)	St. Dev., Pb-rich phase particle diameter, l (mm)	No. of Particles
70	2.0	0.00258	0.00728	4109
70	6.0	0.00273	0.00811	3845
70	10.0	0.00281	0.00821	3307
70	25.8	0.00316	0.00903	3582
70	51.0	0.00313	0.00901	2820
70	90.0	0.00391	0.01099	2225
70	150.0	0.00346	0.00315	3312
70	200.0	0.00359	0.01000	2433
70	350.0	0.00461	0.01306	1648
70	400.0	0.00437	0.01205	1722
100	2.0	0.00334	0.00926	3076
100	6.0	0.00310	0.00881	3147
100	10.0	0.00386	0.01118	1804
100	25.8	0.00396	0.01173	1968
100	51.0	0.00339	0.01014	2384
100	90.0	0.00522	0.01363	1249
100	150.0	0.00472	0.01382	1523
100	200.0	0.00491	0.01368	1354
100	300.0	0.00558	0.01531	1100
100	350.0	0.00543	0.01467	1225
135	3.0	0.00476	0.00494	7625
135	5.1	0.00543	0.00548	6678
135	50.4	0.00542	0.00464	5919
135	101.0	0.00545	0.00496	4771
135	150.0	0.00607	0.00523	3846
135	205.0	0.00726	0.00670	2937
170	1.0	0.00462	0.00468	7729
170	61.3	0.00859	0.00924	2617
170	98.0	0.00974	0.00973	1882
170	149.0	0.01073	0.01368	1723
170	200.0	0.01266	0.01140	1047
170	262.0	0.01127	0.00941	1300
170	317.0	0.01301	0.01097	1068

Table 1

Temperature Category C	Pre-exponential Coefficient, A mm-s$^{1/n}$	Time Exponent, n	Apparent Activation Energy, ΔH kJ/mol
70, 100	3.78×10^{-2}	0.299	23.4
135, 170	0.377	0.195	25.9
70 - 170	7.50×10^{-2}	0.256	23.5

Table 2